Computational Materials Science 165 (2019) 23–33

Contents lists available at ScienceDirect

Computational Materials Science

journal homepage: www.elsevier.com/locate/commatsci

Role of multigrain structure on friction of graphene layers

Huyan Li, Woo Kyun Kim*

Department of Mechanical and Materials Engineering, University of Cincinnati, Cincinnati, OH 45221, USA

ARTICLE INFO

Keywords:
Molecular dynamics
Polycrystalline graphene
Friction

ABSTRACT

Graphene is a one-atom thick two-dimensional material and has a huge potential as a solid lubricant for industrial application. Graphene is often synthesized by chemical vapor deposition (CVD) because of its simplicity and scalability. However, CVD-grown graphene sheets have the multigrain structure, which may have detrimental effects on the superior properties of single-crystal graphene. In particular, the effects of this polycrystalline structure on graphene friction remain far from completely understood. In this study, we investigate the friction between multigrain graphene layers using molecular dynamics (MD) simulations. The MD simulations examine key factors such as grain size and orientation, and morphology of grain boundaries with several different multigrain configurations. The simulation results reveal that multigrain graphene layers exhibit low, but not completely negligible, friction. The observed frictional behaviors are analyzed in terms of the interactions between grains and grain boundaries (GB). In most models, the contribution of the grain-to-grain interaction to the total friction force is negligible, but some grain pairs exhibit relatively large friction if they configure the commensurate interface due to small mismatch in orientation. The interactions involving grain boundaries often exhibit large friction with the largest at the direct GB-to-GB contacts. An analysis shows that the increase in friction near the grain boundary region is directly related to the decrease in interlayer distance, which is caused by the warping of layers in the vicinity of grain boundaries.

1. Introduction

Since it was stably isolated for the first time in 2004 [1], graphene has attracted significant attention in many different fields because of its unique electronic, electrical, mechanical, and thermal properties [2–5]. Apart from these extraordinary properties, graphene is also an excellent solid lubricant which can be coated on various surfaces because of its low surface energy as an atomically thin 2-dimensional material [6,7]. Moreover, graphene provides extreme resistance to wear in various test environments while not posing any adverse effects [8], compared to other solid lubricants. For example, MoS_2 may not last long when oxygen or water molecules are present [9], and graphite and boric acids do not function properly without humidity in the surrounding air [10,11]. Graphene is also proved to be a competitive nanomaterial as an additive in conventional lubricants, such as oils, solvents, and other types of fluids. For example, ethanol-processed graphene layers reduce friction and wear on sliding steel surfaces in air [12]. Some studies also showed that, instead of reducing friction, graphene can increase friction with some modifications such as fluorination [13] or hydrogenation [14]. Therefore, a fundamental understanding of tribological properties of graphene would be of significant importance to various industrial applications.

Several methods have been used to produce graphene, such as mechanical exfoliation [1], epitaxial growth [15], and chemical vapor deposition (CVD) [16]. Among these methods, CVD is most widely used to synthesize high-quality, large-size monolayer graphene films because of its simplicity, low cost, and scalability [17]. Single-atom thick graphene sheets can be produced by CVD at scales of up to meters [18], making their polycrystallinity almost unavoidable, i.e., one graphene film consists of multiple grains of various orientations separated by grain boundaries. Since atoms at grain boundaries are not in perfectly symmetrical conditions and grains have different orientation angles, the properties of polycrystalline graphene may significantly deviate from those of single-crystal graphene. Thus, a number of research efforts have been made to investigate the properties of polycrystalline graphene in various aspects [19–28].

The frictional properties of graphene layers are also affected by the multigrain structure. Some experimental studies on polycrystalline graphene have considered the effects on friction of normal force [13,29–32], number of layers [33,34], humidity [35,36], sliding velocity and wrinkling [37,38], and interface structure between different types of scanning tips and graphene layers on different substrate

* Corresponding author.
E-mail addresses: li2h9@mail.uc.edu (H. Li), kimwu@ucmail.uc.edu (W.K. Kim).

https://doi.org/10.1016/j.commatsci.2019.04.024
Received 5 February 2019; Received in revised form 1 April 2019; Accepted 15 April 2019
Available online 22 April 2019
0927-0256/

materials [31,39–42]. Atomistic computer simulations have also been used to study sliding between graphene layers allowing the direct observation of interacting atoms, for example, between an isolated graphene flake and graphene substrates [32,43–46] or between infinite graphene layers [47]. In particular, Liu et al. [32] showed the effect of incommensurability on friction using tips coated with graphene flakes of different orientation angles. Kavalur and Kim [47] systematically analyzed the effect of grain orientation on friction considering a system consisting of single-crystal graphene and multigrain graphene layers. However, few studies have addressed the sliding friction between polycrystalline graphene layers with arbitrary multigrain structures and the effects of the polycrystalline structure on tribological properties of graphene still remain far from completely understood.

In this research, we used the molecular dynamics methodology to study the roles of multigrain structure in friction of graphene layers and the mechanisms underlying the observations. Our friction models consist of only multigrain layers so that sliding occurs between multigrain layers rather than between the multigrain and single-crystal layers as in [47]. We also analyzed the respective roles of grain and grain boundary in friction by examining key factors such as grain size and orientation, and morphology of grain boundaries with several different multigrain configurations. Our simulation results and analyses revealed main mechanisms causing increase in friction force. The article is structured as follows. In Section 2, we describe the simulation model and structure of multigrain graphene layers used in this study. Section 3 presents the simulation results for friction between multigrain layers and discussion about the physical mechanisms governing the observed frictional behaviors. Finally, Section 4 provides a summary.

2. Models and methods

2.1. Simulation model

Fig. 1 shows a schematic diagram of the simulation model consisting of 4 multigrain graphene layers, labeled layer 1 to layer 4 from bottom to top. Each layer has the dimensions of 200.756 Å × 75.409 Å in the x and y directions. Since the domain size is smaller than real graphene layers in use, periodic boundary conditions are applied in the x and y directions to remove the edge effect, which may be exaggerated otherwise. The bottom layer (layer 1) is fixed in space in order to prevent the rigid body translational motion whereas the top layer (layer 4) moves as a single rigid body, i.e., there is no relative motion between the atoms in layer 4. The two middle layers (layer 2 and layer 3) are comprised of flexible atoms that can move freely in all the three directions, but the atoms at the last row of these layers (red-colored atoms in Fig. 1) are rigidly attached to layer 1 and layer 4, respectively, so that sliding can occur only between layer 2 and layer 3. Layers 1 and 2 are referred to as the bottom substrate and layers 3 and 4 as the top substrate.

This simulation model mimics the AFM experiment so that the top layer (layer 4) represents a graphene layer attached to an AFM tip which is pulled by a cantilever. The deformation of the cantilever was modeled by two linear springs attached at the top layer, which act independently in the x and y directions, as shown in the figure. The spring constants of $k_x = k_y = 5.75$ N/m were adopted from the stiffness of an AFM cantilever [48]. One end of each spring is attached to the center of mass (COM) of the top layer while the other end is connected to two sliders A and B, respectively. During the sliding simulation, slider A moves in the positive x direction with a constant velocity of 1 m/s while slider B remains fixed. The motion of slider A provides a lateral force for the top substrate as the spring length increases and slider B prevents the substantial floating of the top layer in the y direction. As in the AFM experiment where the friction force is measured by the deformation of the cantilever, the extension of the spring attached to slider A was used to calculate the friction force in our simulations. Moreover, the direct measurement of interface forces between layer 2 and later 3 was used in the friction analysis. The total scanning distance is 200.756 Å, which corresponds to one full periodic length of the domain in the x direction. Also, no normal force was externally applied in the z direction.

The interaction of carbon atoms within layers was modeled by the Adaptive Intermolecular Reactive Empirical Bond Order (AIREBO) potential [49] while the Lennard-Jones (L-J) potential was employed for interlayer interactions. The L-J parameters were adopted from Ref. [50]. The multigrain structure was created using the same method as found in [20,47], which will also be explained in the next section. Before sliding simulations begin, the annealing and equilibration processes were applied to obtain stable and reliable grain boundary structures as described in Ref. [47]. The simulations were conducted at 10 K using Langevin thermostat for all free atoms (blue-colored atoms in Fig. 1) [51,52]. This low temperature was chosen to minimize the thermal effect on friction. The simulations were carried out using the Large-scale Atomic/Molecular Massively Parallel Simulator (LAMMPS) program [53] and the post-processing visualizations were performed by Open Visualization Tool (OVITO) [54].

2.2. Multigrain models

A multigrain graphene layer with approximately 6,000 atoms was created using the method proposed in Ref. [20], which was also used in our prior study [47]. In this method grains grow from several initial seed atoms with randomly-chosen orientation angle until they meet each other to form grain boundaries. The orientation angle was measured counterclockwise from the zigzag configuration of single-crystal graphene, where the zigzag and armchair directions correspond to the x and y directions, as illustrated in Fig. 2 (i.e. a positive value is assigned for counterclockwise rotation and vice versa). There are two equivalent zigzag configurations, both of which are illustrated in the figure. Since atoms have three neighbors, three orientation angles are measured for each atom, denoted by θ_1, θ_2, θ_3 (See Fig. 2). Thus, we define the orientation of an atom as the average of θ_1, θ_2, θ_3, i.e., $\frac{1}{3}(\theta_1 + \theta_2 + \theta_3)$. Due to the periodicity in orientation angle, we presented the values in the range of $-30° \sim +30°$. Note that at the initial creation $\theta_1 = \theta_2 = \theta_3$ and the atoms in the same grain have an identical orientation angle. However, after the annealing and equilibration processes, the atoms

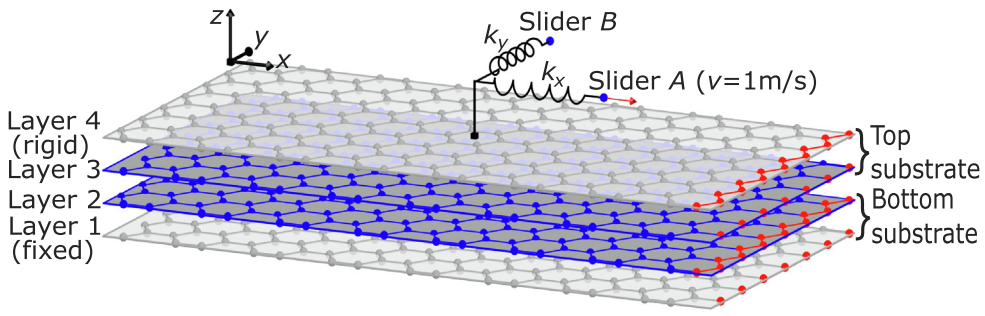

Fig. 1. A schematic diagram of the simulation model consisting of four multigrain graphene layers.

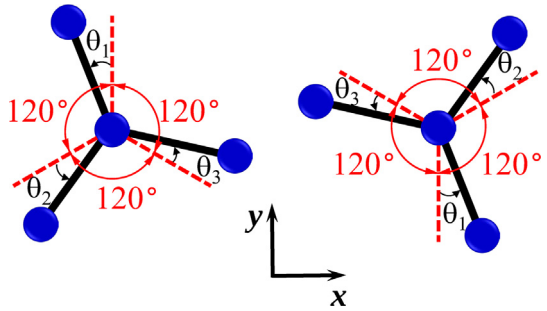

Fig. 2. Definition of orientation angle. Atoms are rotated from the zigzag configuration, represented by the dashed lines, where the zigzag and armchair directions correspond to the x and y directions, respectively. Two equivalent cases are illustrated.

near grain boundaries are deformed so that in general $\theta_1 \neq \theta_2 \neq \theta_3$ and each grain has a non-uniform distribution in orientation angle.

An example configuration of multigrain graphene layer is shown in Fig. 3. As seen in Fig. 3a, each layer has three distinctive regions. We first define the "core" grain boundary region with those atoms which do not form a hexagonal ring, colored red in Fig. 3. Fig. 3b also shows a magnified view near the grain boundary. All the remaining atoms would belong to the grain regions, but those atoms near the core GB regions experience large deformation in terms of both the orientation angle and the elevation (i.e., the z coordinate). In order to maintain the grain region with only those atoms of uniform orientation and elevation, we define an "extended" GB region adjoining the core GB region with the atoms under large deformation, indicated by blue atoms in Fig. 3. Hereinafter, the grain boundary refers to the combined core and extended GB regions unless mentioned otherwise and each grain does not contain any atoms in the extended GB region. Thus, the variations in orientation angle and elevation of atoms in the same grain remain less than $\sim 2°$ and ~ 0.5 Å, respectively.

In this study we prepared four multigrain graphene friction models. First, two distinct multigrain layers with five grains were created for the top and bottom substrates, respectively, as shown in Fig. 4 and then were combined into four friction models. Those five grains in the multigrain layer are labeled t1–t5 for the top substrate and b1–b5 for the bottom substrate, respectively. Note that the grains and core/extended grain boundaries are distinguished in the figures using different colors. Fig. 4 also includes the orientation angle of the grains, which is the averaged value of orientation angles of the individual atoms belonging to the same grain. As seen in Fig. 1, the top and bottom substrates consist of two layers. The second layer in each substrate was obtained by shifting the atom positions in each grain from the first layer according to the A-B stacking and separated from the first layer by an initial equilibrium distance of 3.35 Å. The top and bottom substrates, each of which has two layers, underwent separate equilibration and annealing processes to obtain more stable grain boundary structures. The two substrates were joined to form a sliding model at an average equilibrium distance of 3.35 Å and then a subsequent equilibration with the resultant sliding model was also performed. Detailed conditions of the equilibration and annealing processes are described in Ref. [47].

3. Results and discussion

3.1. Friction force

Fig. 5 shows the friction forces of the four multigrain models, measured using the deformation of the spring as described in Section 2.1, together with the interface forces between layer 2 and layer 3. Note that the interface force was measured with respect to the bottom substrate in accordance with the sign convention of the friction force so that the positive interface force means that the top substrate pulls the bottom substrate in the positive x direction and vice versa. The main graphs include the friction forces for the entire sliding distance of 200.756 Å and the insets have the data for a shorter range of 25 Å. Even though the friction force curves in the main graphs appear very noisy due to the long sliding distance, the insets reveal that there are stick–slip motions during the sliding. Moreover, the two measurements of friction force exhibit close agreement with each other, which justifies using the spring force to represent the friction force in the AFM experiment. This observation also indicates that the sliding velocity used in this study (1 m/s) is low enough to maintain the quasi-static process. As expected from the lack of the uniform periodicity spanning over the entire sliding distance due to the multigrain structure, the stick-slip behaviors displayed in the insets show irregular characteristics in terms of both magnitude of peak force and length of stick events. Hereinafter, the interface force is used to represent the friction force, denoted by f.

As a preliminary step to analyze the role in friction of multigrain structure consisting of grains (GR) and grain boundaries (GB), we tear down the total friction force into the four main contributions; (i) GR-T to GR-B, (ii) GR-T to GB-B, (iii) GB-T to GR-B, and (iv) GB-T to GB-B, where 'T' and 'B' stand for the top and bottom substrates, respectively. Thus, the following relation holds:

$$f_{\text{total}} = f_{\text{GR-T/GR-B}} + f_{\text{GR-T/GB-B}} + f_{\text{GB-T/GR-B}} + f_{\text{GB-T/GB-B}}. \quad (1)$$

The results are shown in Fig. 6. First of all, unlike the total friction force curves, the friction forces of these individual contributions exhibit larger-scale fluctuations, i.e., the overall force curves go up and down over larger sliding distances than the total friction force. Secondly, overall in all models the behaviors of $f_{\text{GR-T/GR-B}}$ and $f_{\text{GR-T/GB-B}}$ are synced with $f_{\text{GB-T/GB-B}}$ and $f_{\text{GB-T/GR-B}}$, respectively, while these two sets of curves fluctuate in the opposite way, i.e., when one goes up the other moves down and vice versa.

This interesting observation can be explained by examining the force map of individual interactions as illustrated in Fig. 7 for model 4. First, Fig. 7a shows the x directional forces of the atoms in the grains on the bottom substrate (GR-B) at a sliding distance of 55 Å which are exerted by those atoms on the grain boundaries of the top substrate (GB-T) with the indication of only positive (blue), negative (red), and zero (green) values. As seen in the figure there are two distinct regions with the positive and negative forces (blue and red) bordered by the

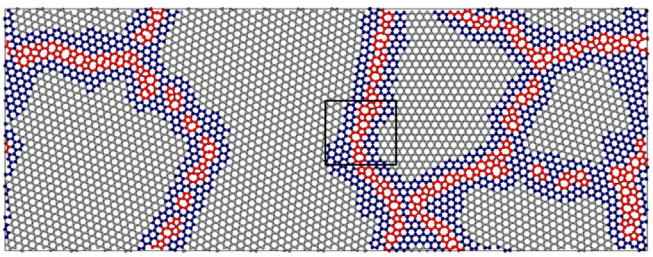

(a) Multigrain structure

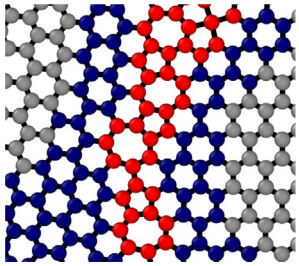

(b) Grain boundary

Fig. 3. Multigrain structure of a graphene layer. Atoms that do not form a hexagonal ring (colored red) comprise the core grain boundary while atoms that form hexagonal rings, but experience large deformation (blue atoms) belong to the extended grain boundary. All the other atoms (colored gray) form the grain regions. (b) shows a more detailed structure of the grain boundary for the region included in the square box in (a).

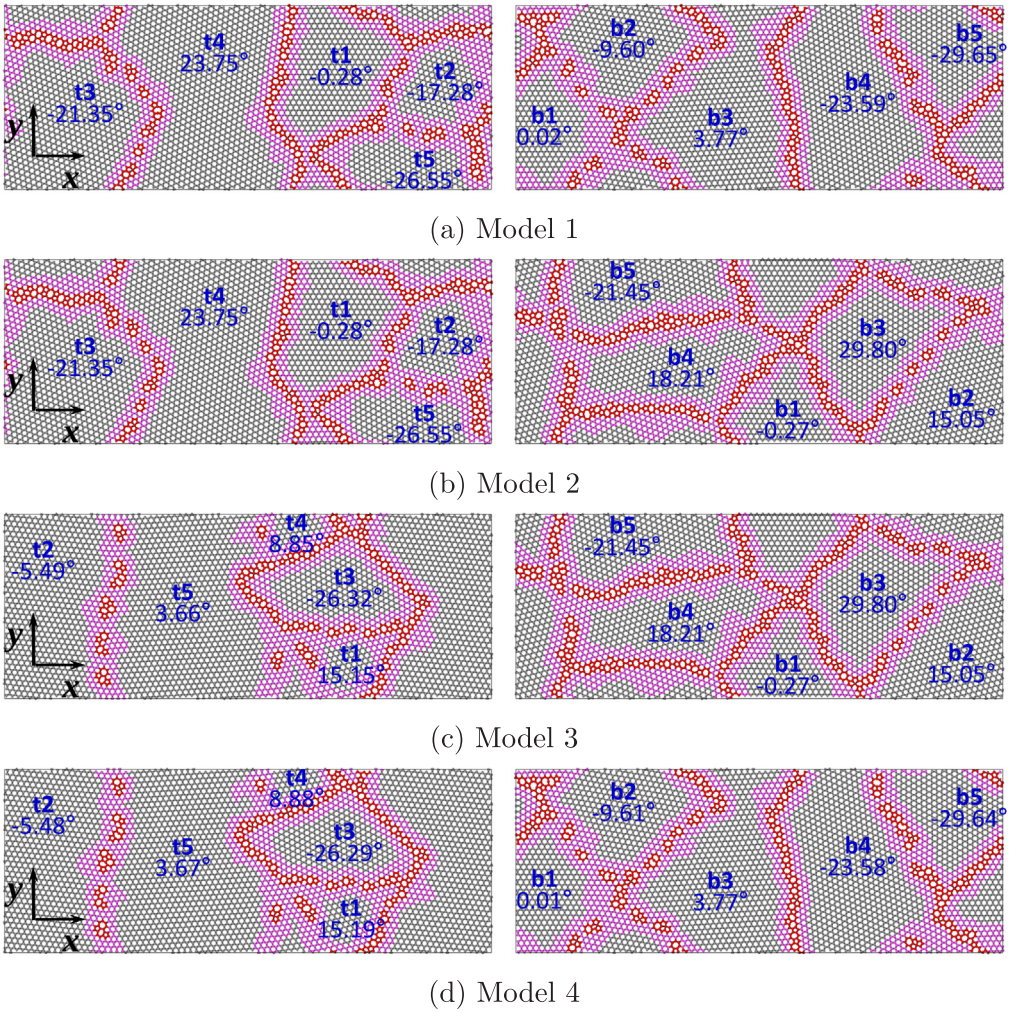

Fig. 4. Atom arrangements of layer 3 (left) and layer 2 (right) of the four models used in sliding simulations. Each layer has 5 grains, denoted by t1–t5 for layer 3 (top substrate) and b1–b5 for layer 2 (bottom substrate). Grains and core/extended grain boundaries are colored differently for better visualization. The rectangular box in each figure represents the periodic domain and the numbers indicate the orientation angle of the corresponding grains (− 30° ∼ +30°).

center-line of the grain boundary between t2 and t5 (See Fig. 4d). Thus, the atoms on the bottom grain located to the right side of the center-line feel the negative force and vice versa, due to the interaction with the top GB. Moreover, those atoms outside of these GB influence regions have zero forces as colored green. Now turning to the forces of the same atoms on the bottom grains, but exerted by the top grain atoms (GR-T), which are illustrated in Fig. 7b, it is seen that the signs of the forces in the influence regions are flipped. That is simply because that the bottom atoms in the (+) region of Fig. 7a now have interacting atoms on the top grains to the more left side of the domain which attract them in the negative x direction. The same explanation can also be applied to those bottom atoms in the (−) region of Fig. 7a. Also, the atoms on the bottom grains which do not have interacting atoms on the top GBs in Fig. 7a now see atoms from the top grains, which is confirmed by the non-green color of the atoms in Fig. 7b. However, these atoms are in general in incommensurate configurations with the top grains, as will be discussed in the next section, so that some atoms feel positive forces while others have negative forces. The net effect is a total force close to zero. Therefore, we have $f_{\text{GR-T/GR-B}} \sim -f_{\text{GB-T/GR-B}}$. In the similar way we can also show that $f_{\text{GR-T/GB-B}} \sim -f_{\text{GB-T/GB-B}}$. In some situations, a majority of atoms can be in the commensurate configuration resulting in the relatively large total force and largest deviation from the synced behaviors.

The total friction force and the four major contributions discussed above are averaged over the sliding distance and shown in Fig. 8a. The two horizontal dashed lines in the figure indicate the minimum (0.042 nN) and maximum (0.41 nN) average friction forces of the pristine-to-multigrain (p-m) graphene models studied in Ref. [47], i.e., one substrate has defect-free single-crystal graphene layers while the other consists of multigrain layers. From our prior study [47] we learned that the friction force of the p-m model is mainly determined by the misorientation angle of grains relative to the pristine layer. That is, the grains that configure the commensurate interfaces with negligible misorientation have larger friction forces. Since the multigrain-to-multigrain (m-m) models have lower probabilities to form commensurate interfaces between grain pairs, we initially expected that the friction force of the m-m models will be smaller than that of the p-m model. However, unlike our initial expectation, the average friction forces of the multigrain-to-multigrain models (0.128 nN ∼ 0.163 nN) are not completely negligible or necessarily smaller than those of the p-m models. Moreover, it was observed that, except for model 4, the GR-T to GR-B interaction has the negligible contribution to the total friction while the contributions from the interactions including GBs in either or both substrates (i.e. GR-T to GB-B, GB-T to GR-B, GB-T to GB-B) are more substantial. These GB contributions to the total friction force are more than 90% in models 1, 2, 3 and more than 70% in model 4. In the next section, we will discuss these observations further with more detailed analysis.

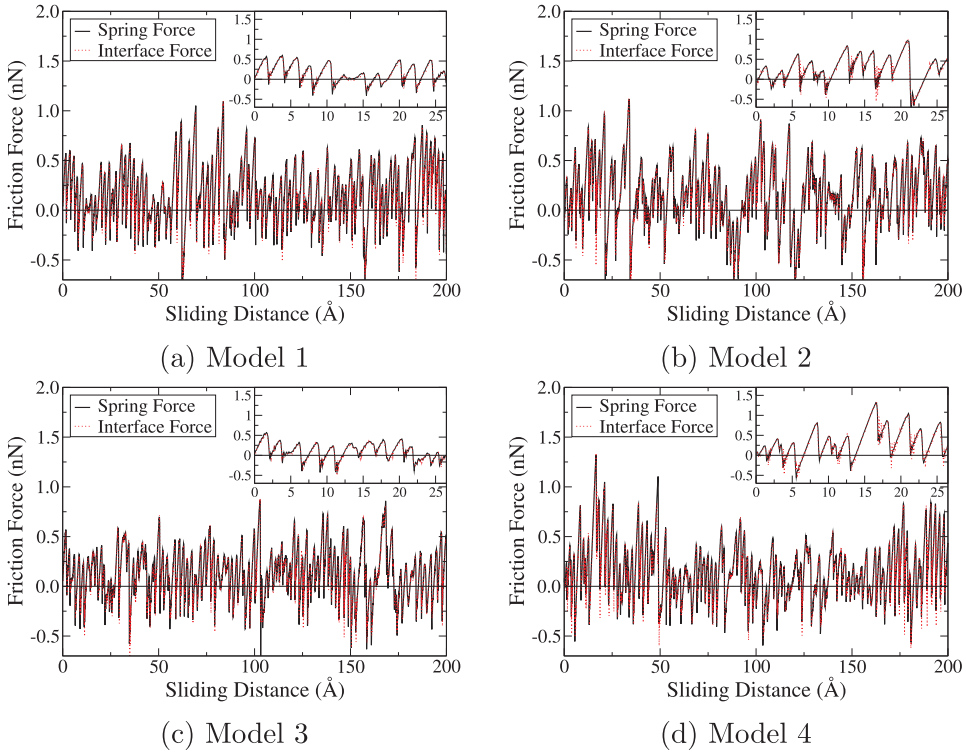

Fig. 5. The friction force calculated by the spring elongation and the interface force between layers 2 and 3 as a function of the sliding distance up to 200.756 Å, which is the periodic domain size in the *x* direction. The insets show the forces for the sliding distance between 0 Å and 25 Å for better visualization.

3.2. Grain-to-grain interactions

We first analyze the effects of the grain-to-grain interaction (GR-T to GR-B) to the friction force. Since there are 5 grains in each substrate, referred to as t1–t5 for the top substrate and b1–b5 for the bottom substrate (See Fig. 4), there are 25 combinations for the interactions between individual grains. Thus,

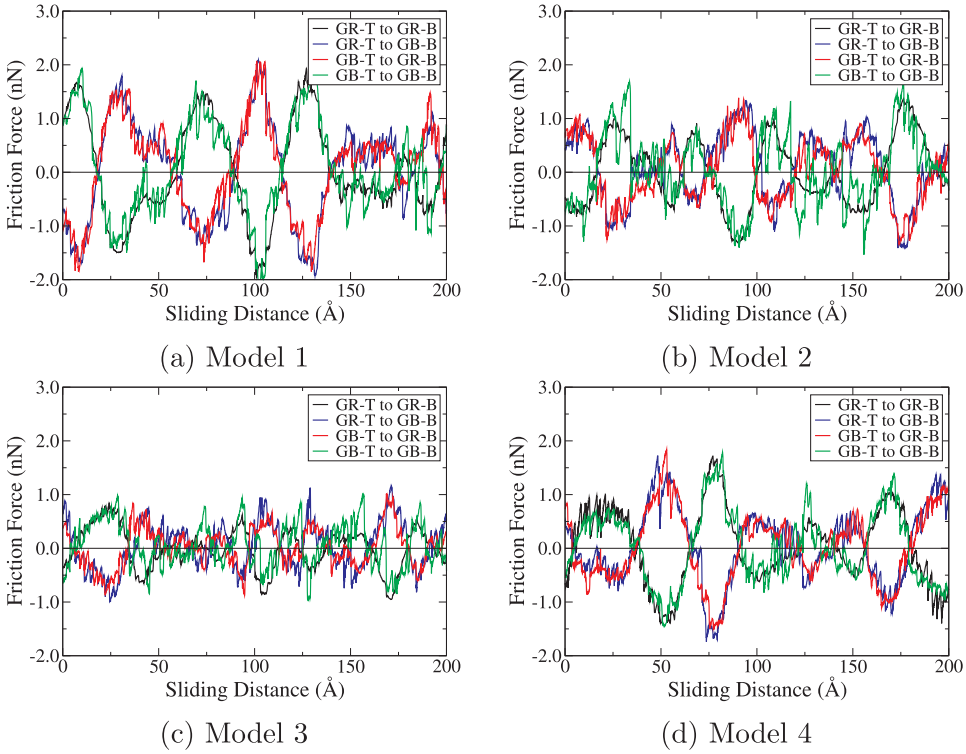

Fig. 6. Contributions to the total friction force of the interactions between grains (GR) and grain boundaries (GB) on the top (T) and bottom (B) substrates, respectively.

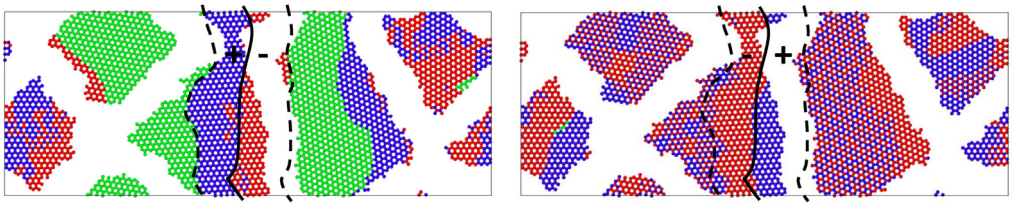

Fig. 7. The interface force map of the grains on the bottom substrate (GR-B) of model 4 at a sliding distance of 55 Å due to the interactions with (a) the grain boundaries (GB-T) and (b) the grains (GR-T) on the top substrate. The blue, red, and green colors indicate the positive, negative, and zero forces, respectively. The solid curve represents the center-line of the grain boundary between t2 and t5 (See Fig. 4d) and the dashed curves indicate the influence range of the GB atoms for both the positive and negative force sides.

$$\begin{aligned} f_{\text{GR-T/GR-B}} = & f_{t1b1} + f_{t1b2} + f_{t1b3} + f_{t1b4} + f_{t1b5} \\ & + f_{t2b1} + f_{t2b2} + f_{t2b3} + f_{t2b4} + f_{t2b5} \\ & + f_{t3b1} + f_{t3b2} + f_{t3b3} + f_{t3b4} + f_{t3b5} \\ & + f_{t4b1} + f_{t4b2} + f_{t4b3} + f_{t4b4} + f_{t4b5} \\ & + f_{t5b1} + f_{t5b2} + f_{t5b3} + f_{t5b4} + f_{t5b5}. \end{aligned} \quad (2)$$

Fig. 9 shows the average friction forces of these 25 combinations for each multigrain model. Most pairs exhibit very low friction as expected from Fig. 8, but there is a particular pair (t5b3) of model 4 with a relatively large friction force. In order to see the effect of misorientation angle between grains (i.e. the difference in orientation angle of two interacting grains) on friction, we plotted the friction forces of all these combinations as a function of misorientation angle in Fig. 10a. As seen in the figure, the t5b3 pair of model 4 has a negligible misorientation angle of − 0.099°, which creates the commensurate configuration between the two grains resulting in the large friction force. Fig. 10a also shows other grain pairs with small misorientation angle, but having lower friction. Since it is also well-known that the friction on atomic scales depends on the actual contact area as well [55,56], the friction force was plotted as a function of overlapping area in Fig. 10b, which was computed by counting the number of atoms in each grain with non-zero force and multiplying it by the area per atom. As seen in the figure, there is little relation between friction force and area. Then, the friction force was normalized by dividing it by the average overlapping area between grains, i.e., we computed the shear strength. The results are shown in Fig. 10c, where the top five grain pairs with the largest shear strength all have small misorientation angles (those enclosed in the dashed ellipse).

However, it is also observed that there are pairs with a very small misorientation angle, but negligible shear strength (e.g. t1b1 of model 2). This behavior can be attributed to the interlocking effect of the multigrain structure. Since each layer has 5 grains surrounded by the grain boundary, a top grain with a very small orientation mismatch relative to a bottom grain may not completely configure the commensurate interface. This explanation is supported by the trajectory of an atom in the top grain plotted against the atom positions in the bottom grain in Fig. 11. In Fig. 11a which shows the t1b1 pair of model 2, the top atom does not exactly follow the local energy minimum path of an assumed commensurate interface, i.e., the path connecting the centers of the honeycomb cells and the atoms located between them in a zigzag fashion, which are indicated by the dashed lines in the figure. On the contrary, the atom in the t5b3 pair of model 4 shown in Fig. 11b moves from one minimum position to another. In short, the small misorientation angle between grains is a necessary condition for large friction, but not a sufficient condition in the multigrain layers.

3.3. Grain boundary effects

Now we turn to the grain boundary effects on friction. As seen in Fig. 8 the contributions of these cases including GBs to the total friction force are more significant than that of the grain-to-grain interactions. Note that, as discussed in Section 3.2, the t5b3 grain pair of model 4 has a large friction force due to the small misorientation angle so that the contribution from the grain-to-grain interactions of model 4 is relatively larger than the other models.

We consider the GB effects in terms of three categories; (i) GR-T to GB-B, the interaction between the grains on the top substrate (t1 ~ t5) and the grain boundaries on the bottom substrate, (ii) GB-T to GR-B, the interaction between the grain boundaries on the top substrate and the grains on the bottom substrate (b1 ~ b5), and (iii) GB-T to GB-B, the interaction between the grain boundaries of the top and bottom substrates. Thus, the following relations hold.

$$f_{\text{GR-T/GB-B}} = f_{t1/\text{GB-B}} + f_{t2/\text{GB-B}} + f_{t3/\text{GB-B}} + f_{t4/\text{GB-B}} + f_{t5/\text{GB-B}}, \quad (3)$$

$$f_{\text{GB-T/GR-B}} = f_{\text{GB-T/b1}} + f_{\text{GB-T/b2}} + f_{\text{GB-T/b3}} + f_{\text{GB-T/b4}} + f_{\text{GB-T/b5}}. \quad (4)$$

The friction force results of these cases are shown in Fig. 12, where the interactions with both the core GB and extended GB regions and with only the core GB regions are included as open and filled circles and squares, respectively. In many cases, there is no significant difference in

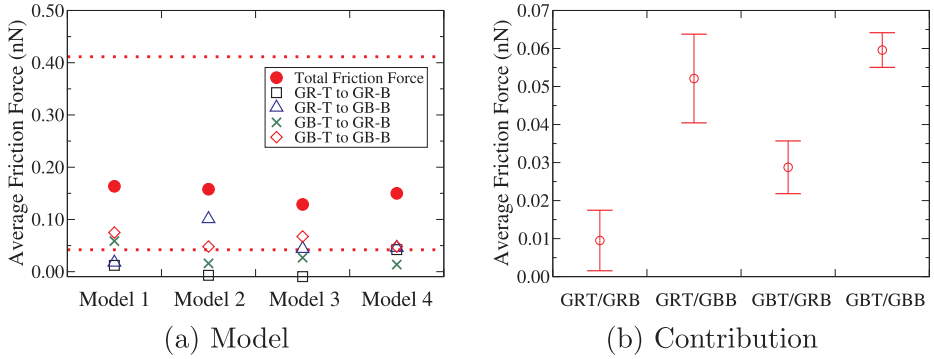

Fig. 8. Average friction forces shown (a) for each model and (b) for each contribution. The two horizontal dashed lines in (a) show the minimum and maximum friction forces of the pristine-to-multigrain models studied in Ref. [47] and the error bars in (b) indicate the standard errors.

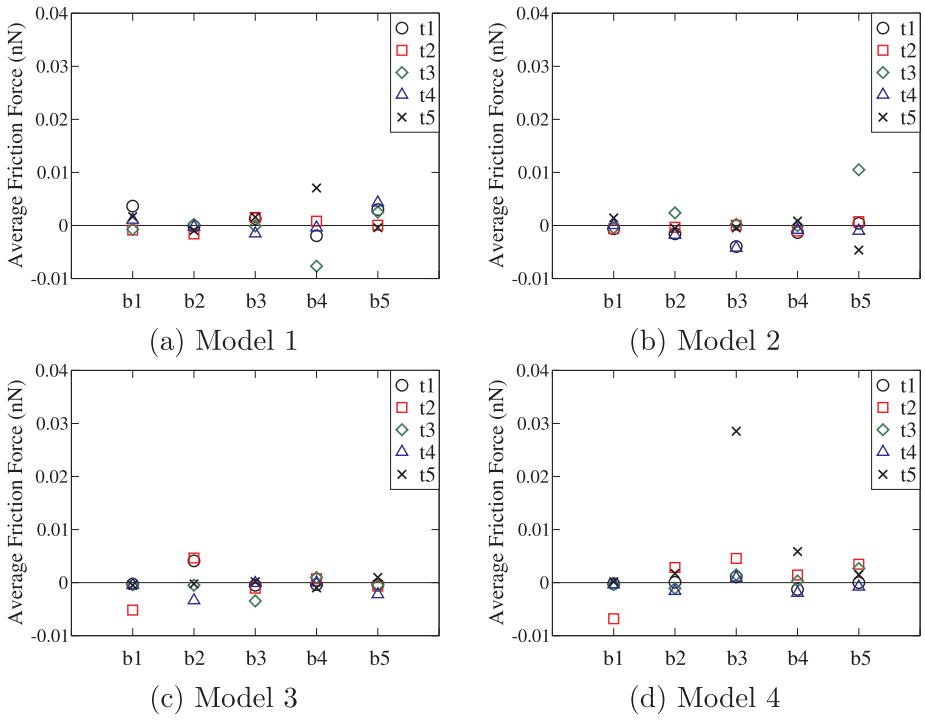

Fig. 9. Average friction force between a pair of grains in layer 2 and layer 3. t1–t5 denote the grains in layer 3 (the top substrate) and b1–b5 denote the grains in layer 2 (the bottom substrate).

friction force between the two definitions of GB, implying that the core GBs have stronger interactions with grains than the extended GBs. However, in models 3 and 4 there are cases where the effects from the extended GBs are not trivial. We will revisit this issue later after discussing the GB-to-GB interaction. It is also apparent that the friction force due to the direct GB-to-GB interaction is the largest in all the models. For comparison, the figure also shows the friction forces of the grain-to-grain interactions as vertical bars to the left and right of the GB results. Each bar extends between the minimum and maximum forces among all the grain pairs including a particular grain indicated by the

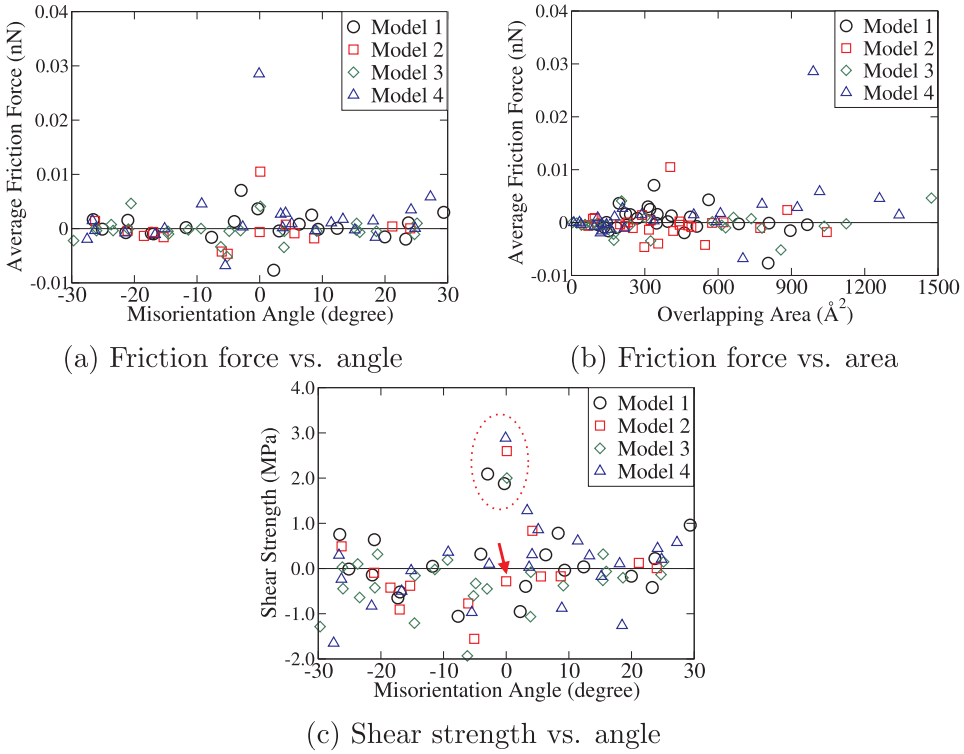

Fig. 10. The friction force as functions of (a) misorientation angle and (b) overlapping area. The shear strength is also shown as a function of misorientation angle in (c). The grain pairs inside the dashed ellipse in (c) are t1b1 (– 0.29°), t5b4 (– 2.96°) of model 1, t3b5 (0.090°) of model 2, t1b2 (0.11°) of model 3, and t5b3 (– 0.099°) of model 4. The arrow indicates t1b1 (0.0077°) of model 2.

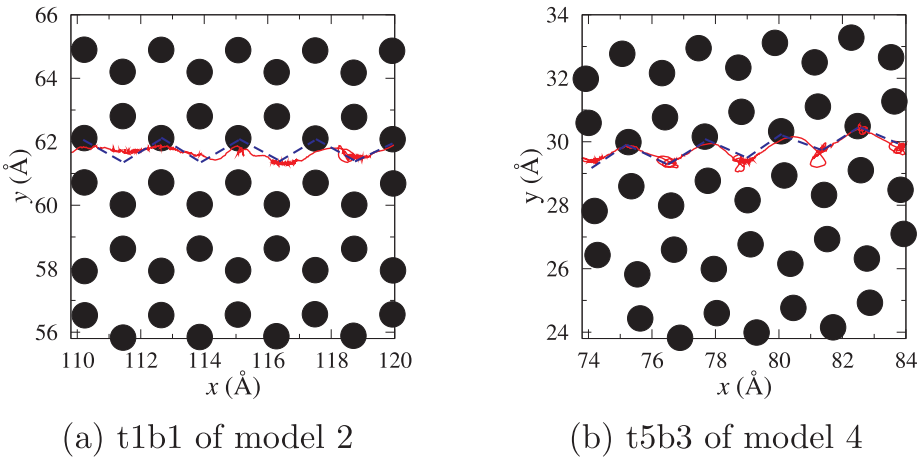

Fig. 11. The trajectory of an atom in the top substrate. The filled circles represent the mean positions of atoms in the bottom grain. The dashed lines show local energy minimum paths when a commensurate interface is formed.

bar heading. In most cases each grain, whether on the top substrate or on the bottom substrate, has larger friction forces due to the interaction with GBs than the interactions with the other grains. Again, a noticeable exception is model 4, where t5 and b3 have larger friction forces due to the interaction with each other than the interaction with GBs.

Since the core GB regions consist of only non-hexagonal rings with random orientation angles, as shown in Fig. 3b, misorientation cannot explain this phenomenon unlike the grain-to-grain interactions. Thus, other mechanisms should be found that are attributed to this increase in friction of GB regions. Fig. 13 shows the side view of the multigrain models with atoms in the core GB, extended GB, and grain regions colored differently. As seen in the figures, the atoms in the grain boundary regions are displaced vertically so that the interlayer distance between the top and bottom substrates becomes smaller in the GB regions than in the grain regions, which is most apparent in the core GB regions (See the red atoms in Fig. 13). The direct relation between the interlayer distance and friction force is seen in Fig. 14, which shows the friction forces as functions of the reciprocal of the minimum atomic distance for each pair (GR-GB or GB-GB) during sliding. The figure also includes the results for grain-to-grain interactions. Except for t5b3 of model 4, grain pairs have larger distances and therefore negligible friction forces. For the pairs including GBs at least on one substrate, there is an overall trend that the friction force increases with decreasing interlayer distance. Because of the interlocking effect of the multigrain structure, mentioned in Section 3.2, there are some pairs with negligible friction even with smaller interlayer distance.

Next, we discuss more details of the GB-to-GB interaction, which exhibits the largest friction force. According to our definition, the grain boundary consists of the core GB and extended GB regions (See Fig. 3). Thus,

$$f_{\text{GB-T/GB-B}} = f_{\text{core GB-T/core GB-B}} + f_{\text{core GB-T/extended GB-B}} + f_{\text{extended GB-T/core GB-B}} + f_{\text{extended GB-T/extended GB-B}}. \quad (5)$$

Their individual effect on friction force is shown in Fig. 15a, where each model exhibits very different trends. Model 1 and model 4 have the largest friction force between the core GB regions on the top and

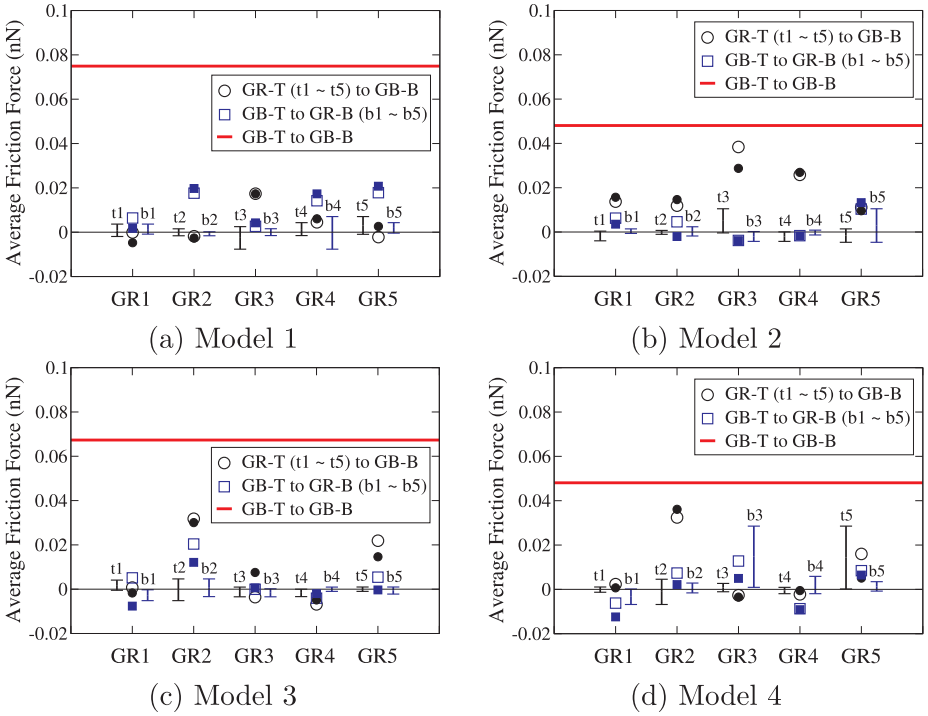

Fig. 12. The average friction force of the multigrain models. GR 1 to GR 5 refer to either t1–t5 for GR-T to GB-B or b1–b5 for GB-T to GR-B. The open circles and squares represent the interactions considering both the core and extended GB atoms while the filled circles and squares show the friction forces only due to the core GB atoms. For comparison, the friction forces of the grain-to-grain interactions are also included to the left and right of the GB results as vertical bars. Each bar shows the minimum and maximum friction forces of the grain pairs including a particular grain indicated by the bar heading. E.g., the bar graph with heading 't1' extends between the minimum and maximum forces among all the grain pairs including t1 (t1b1, t1b2, t1b3, t1b4, t1b5).

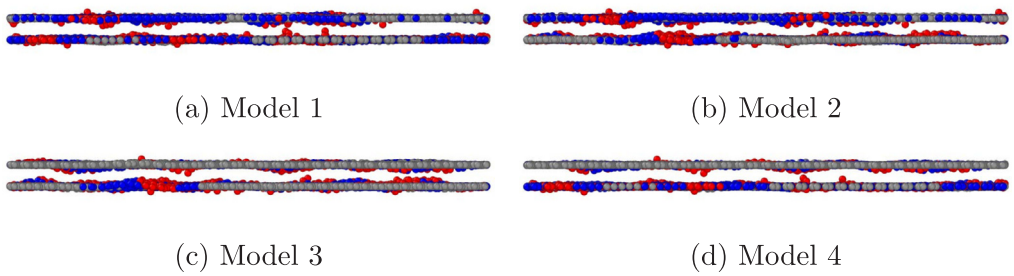

Fig. 13. The side view of multigrain layers 2 and 3. Red, blue, and gray atoms represent the core GB, extended GB and grain atoms, respectively.

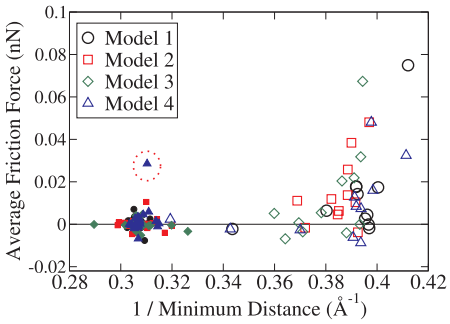

Fig. 14. The friction force as a function of the reciprocal of the minimum distance between atom pairs. Open objects are for each GB case in Fig. 12 and closed objects represent the results for the grain pairs shown in Fig. 9. The data point inside the dashed circle is for t5b3 of model 4.

bottom substrates while the friction force between the core GB and extended GB regions are the largest in model 2 and model 3. As in Fig. 14, we plotted the friction force of this case using the reciprocal of the minimum distance, shown in Fig. 15b. Overall, the pairs with the smaller interlayer distance have larger friction forces although each model has the minimum distance at different pairs. For example, in model 1 the core GBs has the minimum distance during the sliding while model 2 has the minimum distance at the pair of core GB-T and extended GB-B. The main difference of the direct GB-to-GB interaction from all the other pairs is that in the GB-to-GB case there is no grain on both substrates so that the contact happens between two vertically-warped lines rather than the line-to-flat area contact as in the cases including grains. These line-to-line contacts in the various GB-GB cases create a very complex topology, resulting in the friction force trend shown in Fig. 15a.

Finally, we discuss the respective effects of the core GB and extended GB to the total friction force by defining the core GB force and extended GB force as

$$f_{\text{core GB}} = f_{\text{core GB-T/GR-B}} + f_{\text{GR-T/core GB-B}} + f_{\text{core GB-T/core GB-B}} + 0.5 \times (f_{\text{core GB-T/extended GB-B}} + f_{\text{extended GB-T/core GB-B}}), \quad (6)$$

$$f_{\text{extended GB}} = f_{\text{extended GB-T/GR-B}} + f_{\text{GR-T/extended GB-B}} + f_{\text{extended GB-T/extended GB-B}} + 0.5 \times (f_{\text{core GB-T/extended GB-B}} + f_{\text{extended GB-T/core GB-B}}). \quad (7)$$

Note that to avoid duplication only the half of the interactions between the core GB and the extended GB was added to each force. The results are shown in Fig. 16. In models 1 and 2 the core GB has dominant effects on friction force while both the core and extended GB regions play important roles in friction in models 3 and 4. As we discussed above, the main mechanism attributed to increase in friction with GB regions is the change in topology near the GB regions which decreases the interlayer distance. Moreover, the graph in Fig. 16 suggests that not only the core GB, but also the extended GB regions should be taken into account to explain the frictional behaviors of multigrain graphene layers.

4. Conclusion

We studied the role of multigrain structure on friction of polycrystalline graphene using molecular dynamics simulations. The four distinct multigrain sliding models were constructed by joining multigrain graphene layers, each of which contains five grains of random orientation, separated by grain boundaries. The sliding simulation mimicked the AFM experiment so that the rigid top layer was pulled by a slider moving at a constant velocity via a linear spring modeling the elastic deformation of the AFM cantilever. The friction force was measured by the spring extension and the interlayer interactions between graphene layers. Both exhibited close agreement with each other and the latter was used to analyze the simulation results.

The friction force results exhibited irregular stick-slip behaviors due to the lack of periodicity of the multigrain structure. Moreover, the average friction force of these multigrain-to-multigrain models was not

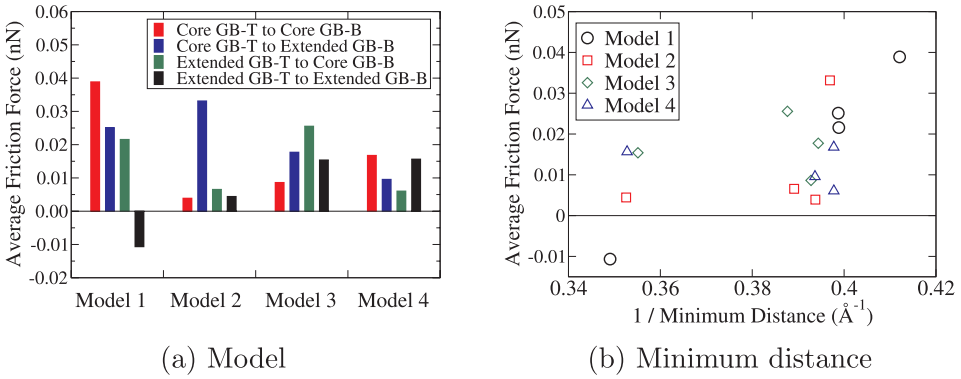

Fig. 15. The average friction force of the interaction between the core and extended GB regions. The average friction forces including the interactions between the core and extended GB regions are shown in (a). These friction forces are also shown as a function of the reciprocal of the minimum distance between pairs in (b).

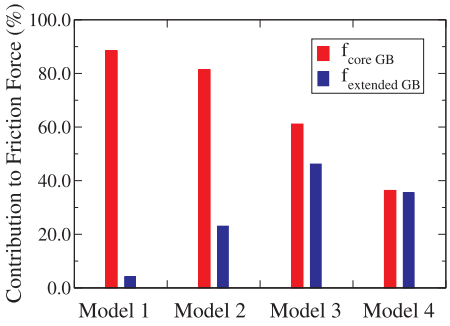

Fig. 16. The contributions of the core GB and extended GB forces to the total friction force.

completely negligible, but took values between the minimum and maximum friction forces of the single-crystal-to-multigrain layers [47]. In order to analyze the individual effects of grains and grain boundaries on friction, the total friction force was separated out into the four contributions; (i) GR-T to GR-B, (ii) GR-T to GB-B, (iii) GB-T to GR-B, and (iv) GB-T to GB-B. It was observed that the GR-T to GR-B interaction had negligible contributions while the interactions including grain boundaries on at least one substrate had more substantial effects on friction. These GB contributions were responsible for more than 90% in models 1, 2, 3 and for more than 70% in model 4 of the total friction force.

The contribution of the grain-to-grain (GR-T to GR-B) interactions to the total friction force was further discussed by considering individual grain pairs formed with the respective grains of the top and bottom substrates. While most of the grain pairs exhibited negligible friction, some had relatively large friction forces because of the small misorientation angle configuring the commensurate interface between grains. In order to separate out the area effect, the shear strength defined as the friction force per unit overlapping area was also computed for all pairs. It was found that all the pairs experiencing large shear strength had small orientation angles, but there also existed some pairs even with small misorientation, but negligible friction due to the interlocking effect of the multigrain structure preventing the commensurate interface.

The grain boundary effects on friction, which are the main causes of the non-trivial friction force of the multigrain graphene layers, were analyzed by considering three distinct contributions; GR-T to GB-B, GB-T to GR-B, and GB-T to GB-B. In most cases the friction forces between grains and grain boundaries (i.e. GR-T to GB-B or GB-T to GR-B) are larger than the corresponding grain-to-grain interactions with a noticeable exception of grains t5 and b3 in model 4 with the largest friction force at the direct GB-to-GB contact. Also, it was observed that the core GB atoms have dominant effects on friction force in the interaction with grains, compared to the extended GB atoms. This increase in friction can be attributed to the reduced interlayer distance in the GB regions where atoms are displaced in the vertical direction. The direct GB-to-GB interaction was further analyzed in terms of the interactions between the core and extended GB regions. While the same overall trend between the friction force and interlayer distance was observed, there was no consistent observation in the combination that has the largest friction force. For example, in model 1 the core GB-to-core GB interaction exhibited the largest friction force while in model 2 it occurred between the core GB and extended GB regions. This behavior was mainly due to the complex topology of the line-to-line contact between the grain boundaries where atoms on both substrates are severely displaced.

CRediT authorship contribution statement

Huyan Li: Conceptualization, Data curation, Formal analysis, Methodology, Validation, Visualization, Writing - original draft, Writing - review & editing, Software. **Woo Kyun Kim:** Conceptualization, Data curation, Formal analysis, Methodology, Validation, Visualization, Writing - original draft, Writing - review & editing, Software, Funding acquisition, Project administration, Supervision.

Acknowledgment

This work was supported in part by the National Science Foundation under Award Number 1662666.

Data availability

The raw/processed data required to reproduce these findings cannot be shared at this time as the data also forms part of an ongoing study.

Appendix A. Supplementary data

Supplementary data associated with this article can be found, in the online version, at https://doi.org/10.1016/j.commatsci.2019.04.024.

References

[1] K.S. Novoselov, A.K. Geim, S.V. Morozov, D. Jiang, Y. Zhang, S.V. Dubonos, I.V. Grigorieva, A.A. Firsov, Electric field effect in atomically thin carbon films, Science 306 (5696) (2004) 666–669.
[2] T.C. Nguyen, M. Otani, S. Okada, Semiconducting electronic property of graphene adsorbed on (0001) surfaces of SiO2, Phys. Rev. Lett. 106 (10) (2011) 106801 .
[3] K. Kim, H.J. Park, B.-C. Woo, K.J. Kim, G.T. Kim, W.S. Yun, Electric property evolution of structurally defected multilayer graphene, Nano Lett. 8 (10) (2008) 3092–3096.
[4] I. Frank, D.M. Tanenbaum, A.M. van der Zande, P.L. McEuen, Mechanical properties of suspended graphene sheets, J. Vacuum Sci. Technol. B 25 (6) (2007) 2558–2561.
[5] A.A. Balandin, S. Ghosh, W. Bao, I. Calizo, D. Teweldebrhan, F. Miao, C.N. Lau, Superior thermal conductivity of single-layer graphene, Nano Lett. 8 (3) (2008) 902–907.
[6] S.H. Kim, D.B. Asay, M.T. Dugger, Nanotribology and MEMS, Nano Today 2 (5) (2007) 22–29.
[7] R. Maboudian, W.R. Ashurst, C. Carraro, Tribological challenges in micro-mechanical systems, Tribol. Lett. 12 (2) (2002) 95–100.
[8] D. Berman, A. Erdemir, A.V. Sumant, Graphene: a new emerging lubricant, Mater. Today 17 (1) (2014) 31–42.
[9] J. Lancaster, A review of the influence of environmental humidity and water on friction, lubrication and wear, Tribol. Int. 23 (6) (1990) 371–389.
[10] G. Rowe, Some observations on the frictional behaviour of boron nitride and of graphite, Wear 3 (4) (1960) 274–285.
[11] A. Erdemir, O. Eryilmaz, G. Fenske, Self-replenishing solid lubricant films on boron carbide, Surf. Eng. 15 (4) (1999) 291–295.
[12] D. Berman, A. Erdemir, A.V. Sumant, Few layer graphene to reduce wear and friction on sliding steel surfaces, Carbon 54 (2013) 454–459.
[13] S. Kwon, J.-H. Ko, K.-J. Jeon, Y.-H. Kim, J.Y. Park, Enhanced nanoscale friction on fluorinated graphene, Nano Lett. 12 (12) (2012) 6043–6048.
[14] Y. Dong, X. Wu, A. Martini, Atomic roughness enhanced friction on hydrogenated graphene, Nanotechnology 24 (37) (2013) 375701 .
[15] P.W. Sutter, J.-I. Flege, E.A. Sutter, Epitaxial graphene on ruthenium, Nat. Mater. 7 (5) (2008) 406.
[16] K.S. Kim, Y. Zhao, H. Jang, S.Y. Lee, J.M. Kim, K.S. Kim, J.-H. Ahn, P. Kim, J.-Y. Choi, B.H. Hong, Large-scale pattern growth of graphene films for stretchable transparent electrodes, Nature 457 (7230) (2009) 706.
[17] X. Li, W. Cai, J. An, S. Kim, J. Nah, D. Yang, R. Piner, A. Velamakanni, I. Jung, E. Tutuc, et al., Large-area synthesis of high-quality and uniform graphene films on copper foils, Science 324 (5932) (2009) 1312–1314.
[18] S. Bae, H. Kim, Y. Lee, X. Xu, J.-S. Park, Y. Zheng, J. Balakrishnan, T. Lei, H.R. Kim, Y.I. Song, et al., Roll-to-roll production of 30-inch graphene films for transparent electrodes, Nat. Nanotechnol. 5 (8) (2010) 574.
[19] R. Grantab, V.B. Shenoy, R.S. Ruoff, Anomalous strength characteristics of tilt grain boundaries in graphene, Science 330 (6006) (2010) 946–948.
[20] J. Kotakoski, J.C. Meyer, Mechanical properties of polycrystalline graphene based on a realistic atomistic model, Phys. Rev. B 85 (19) (2012) 195447 .
[21] O.V. Yazyev, Polycrystalline graphene: atomic structure, energetics and transport properties, Solid State Commun. 152 (15) (2012) 1431–1436.
[22] J. Zhang, J. Zhao, Structures and electronic properties of symmetric and nonsymmetric graphene grain boundaries, Carbon 55 (2013) 151–159.
[23] Z. Song, V.I. Artyukhov, B.I. Yakobson, Z. Xu, Pseudo Hall-Petch strength reduction in polycrystalline graphene, Nano Lett. 13 (4) (2013) 1829–1833.

[24] B. Wang, Y.S. Puzyrev, S.T. Pantelides, Enhanced chemical reactions of oxygen at grain boundaries in polycrystalline graphene, Polyhedron 64 (2013) 158–162.
[25] H. Liu, Y. Lin, S. Luo, Grain boundary energy and grain size dependences of thermal conductivity of polycrystalline graphene, J. Phys. Chem. C 118 (42) (2014) 24797–24802.
[26] B. Mortazavi, G. Cuniberti, Atomistic modeling of mechanical properties of polycrystalline graphene, Nanotechnology 25 (21) (2014) 215704 .
[27] M. Chen, S. Quek, Z. Sha, C. Chiu, Q. Pei, Y. Zhang, Effects of grain size, temperature and strain rate on the mechanical properties of polycrystalline graphene – a molecular dynamics study, Carbon 85 (2015) 135–146.
[28] M. Becton, X. Zeng, X. Wang, Computational study on the effects of annealing on the mechanical properties of polycrystalline graphene, Carbon 86 (2015) 338–349.
[29] K.-S. Kim, H.-J. Lee, C. Lee, S.-K. Lee, H. Jang, J.-H. Ahn, J.-H. Kim, H.-J. Lee, Chemical vapor deposition-grown graphene: the thinnest solid lubricant, ACS Nano 5 (6) (2011) 5107–5114.
[30] Z. Ye, P. Egberts, G.H. Han, A.C. Johnson, R.W. Carpick, A. Martini, Load-dependent friction hysteresis on graphene, ACS Nano 10 (5) (2016) 5161–5168.
[31] P. Egberts, G.H. Han, X.Z. Liu, A.C. Johnson, R.W. Carpick, Frictional behavior of atomically thin sheets: hexagonal-shaped graphene islands grown on copper by chemical vapor deposition, ACS Nano 8 (5) (2014) 5010–5021.
[32] S.-W. Liu, H.-P. Wang, Q. Xu, T.-B. Ma, G. Yu, C. Zhang, D. Geng, Z. Yu, S. Zhang, W. Wang, et al., Robust microscale superlubricity under high contact pressure enabled by graphene-coated microsphere, Nat. Commun. 8 (2017) 14029.
[33] Y. Huang, Q. Yao, Y. Qi, Y. Cheng, H. Wang, Q. Li, Y. Meng, Wear evolution of monolayer graphene at the macroscale, Carbon 115 (2017) 600–607.
[34] M. Tripathi, F. Awaja, G. Paolicelli, R. Bartali, E. Iacob, S. Valeri, S. Ryu, S. Signetti, G. Speranza, N.M. Pugno, Tribological characteristics of few-layer graphene over Ni grain and interface boundaries, Nanoscale 8 (12) (2016) 6646–6658.
[35] S. Bhowmick, A. Banerji, A.T. Alpas, Role of humidity in reducing sliding friction of multilayered graphene, Carbon 87 (2015) 374–384.
[36] J. Vilhena, C. Pimentel, P. Pedraz, F. Luo, P.A. Serena, C.M. Pina, E. Gnecco, R. Peerez, Atomic-scale sliding friction on graphene in water, ACS Nano 10 (4) (2016) 4288–4293.
[37] W.-K. Lee, M. Haydell, J.T. Robinson, A.R. Laracuente, E. Cimpoiasu, W.P. King, P.E. Sheehan, Nanoscale reduction of graphene fluoride via thermochemical nanolithography, ACS Nano 7 (7) (2013) 6219–6224.
[38] F. Long, P. Yasaei, W. Yao, A. Salehi-Khojin, R. Shahbazian-Yassar, Anisotropic friction of wrinkled graphene grown by chemical vapor deposition, ACS Appl. Mater. Interfaces 9 (24) (2017) 20922–20927.
[39] G. Paolicelli, M. Tripathi, V. Corradini, A. Candini, S. Valeri, Nanoscale frictional behavior of graphene on SiO2 and Ni (111) substrates, Nanotechnology 26 (5) (2015) 055703 .
[40] D. Berman, A. Erdemir, A.V. Zinovev, A.V. Sumant, Nanoscale friction properties of graphene and graphene oxide, Diam. Relat. Mater. 54 (2015) 91–96.
[41] L. Kolodziejczyk, P. Kula, W. Szymanski, R. Atraszkiewicz, K. Dybowski, R. Pietrasik, Frictional behaviour of polycrystalline graphene grown on liquid metallic matrix, Tribol. Int. 93 (2016) 628–639.
[42] S. Bhowmick, A. Banerji, A. Alpas, Friction reduction mechanisms in multilayer graphene sliding against hydrogenated diamond-like carbon, Carbon 109 (2016) 795–804.
[43] F. Bonelli, N. Manini, E. Cadelano, L. Colombo, Atomistic simulations of the sliding friction of graphene flakes, Eur. Phys. J. B 70 (4) (2009) 449–459.
[44] Y. Guo, W. Guo, C. Chen, Modifying atomic-scale friction between two graphene sheets: a molecular-force-field study, Phys. Rev. B 76 (15) (2007) 155429 .
[45] H.M. Yoon, S. Kondaraju, J.S. Lee, Molecular dynamics simulations of the friction experienced by graphene flakes in rotational motion, Tribol. Int. 70 (2014) 170–178.
[46] M. Van Wijk, M. Dienwiebel, J. Frenken, A. Fasolino, Superlubric to stick-slip sliding of incommensurate graphene flakes on graphite, Phys. Rev. B 88 (23) (2013) 235423 .
[47] A. Kavalur, W.K. Kim, Molecular dynamics study on friction of polycrystalline graphene, Comput. Mater. Sci. 137 (2017) 346–361.
[48] M. Dienwiebel, G.S. Verhoeven, N. Pradeep, J.W. Frenken, J.A. Heimberg, H.W. Zandbergen, Superlubricity of graphite, Phys. Rev. Lett. 92 (12) (2004) 126101 .
[49] S.J. Stuart, A.B. Tutein, J.A. Harrison, A reactive potential for hydrocarbons with intermolecular interactions, J. Chem. Phys. 112 (2000) (2000) 6472–6486 ISSN 00219606.
[50] Y. Shibuta, J.A. Elliott, Interaction between two graphene sheets with a turbostratic orientational relationship, Chem. Phys. Lett. 512 (4–6) (2011) 146–150.
[51] T. Schneider, E. Stoll, Molecular-dynamics study of a three-dimensional one-component model for distortive phase transitions, Phys. Rev. B 17 (3) (1978) 1302.
[52] B. Dünweg, W. Paul, Brownian dynamics simulations without Gaussian random numbers, Int. J. Mod. Phys. C 2 (03) (1991) 817–827.
[53] S. Plimpton, Fast parallel algorithms for short – range molecular dynamics, J. Comput. Phys. 117 (1994) (1995) 1–19 ISSN 00219991.http://lammps.sandia.gov.
[54] A. Stukowski, Visualization and analysis of atomistic simulation data with OVITO–the Open Visualization Tool, Modell. Simul. Mater. Sci. Eng. 18 (1) (2009) 015012 ISSN 0965-0393.
[55] M. Enachescu, R. Van den Oetelaar, R. Carpick, D. Ogletree, C. Flipse, M. Salmeron, Observation of proportionality between friction and contact area at the nanometer scale, Tribol. Lett. 7 (2–3) (1999) 73.
[56] Y. Mo, K.T. Turner, I. Szlufarska, Friction laws at the nanoscale, Nature 457 (7233) (2009) 1116.